Available online at www.sciencedirect.com

SciVerse ScienceDirect

Ceramics International 39 (2013) 2023–2030

CERAMICS INTERNATIONAL

www.elsevier.com/locate/ceramint

Biaxial flexural strength of poled lead zirconate titanate under high electric field with extended field range ☆

Kewei Zhang, Fan Wen Zeng, Hong Wang*, Hua-Tay Lin

Materials Science and Technology Division, Oak Ridge National Laboratory, 1Bethel Valley Road, Oak Ridge, TN 37831-6069, USA

Received 6 June 2012; received in revised form 15 August 2012; accepted 16 August 2012
Available online 23 August 2012

Abstract

In the present work, as-received poled lead zirconate titanate, or PZT, was examined using ball-on-ring (BoR) mechanical testing coupled with an electric field. Electric fields in the range of $\pm 4E_C$ (E_C, coercive field) with controlled loading paths were applied, and mechanical tests at a substantial number of characteristic electric field levels were conducted. Commercial electronic liquid FC-40 was used to prevent the setup from dielectric breakdown under a high electric field. Weibull strength distribution was used to interpret the mechanical strength data. The data showed that the strength levels of the PZT tested under OC (open circuit) in air and in FC-40 were almost the same. It was further revealed that, for the studied cases, the effect of loading history on the biaxial flexural strength of the PZT was significant in $-E_C$, but not in OC or zero field as well as $4E_C$. An asymmetric "V" curve was observed for the characteristic strength-electric field graph, and the bottom of "V" curve was located near the negative coercive field. Microscopic analysis showed that surface-located volume-distributed flaws were the strength limiter and responsible for the failure of the tested PZT under electromechanical loadings.

Keywords: C. Fracture; C. Strength; D. PZT

1. Introduction

High piezoelectric coefficients and high Curie temperatures are key performance requirements for piezoelectric ceramics that are used in a piezo-fuel injector. Lead zirconate titanate, or PZT, meets these requirements and is consequently considered to be a great candidate for such applications [1]. It has been demonstrated that a PZT actuator-based fuel injection system can effectively reduce fuel consumption, pollutants such as NO_x, and engine noise [2]. However, the low fracture toughness of PZT ($\sim$1 MPa $m^{1/2}$) [3,4] becomes a major concern upon application.

Over the last several decades, much effort has been focused on studying the failure mechanism of PZT actuators. The strain mismatch between the electrically active and inactive regions was found to be responsible for most of the degradations and failures of PZT actuators [5]. Though PZT actuators with different designs have been developed to minimize the strain mismatch [6], the potential for cracking cannot be eliminated. Preexisting flaws obviously play an important role in crack initiation and growth within the PZT. Furthermore, the preexisting flaws can be easily introduced during the fabrication process, which involves sintering, casting, lamination, cutting, and poling [7]. Various testing methods such as indentation [8–10], impact tension [11–17], three- [18–20] or four-point [21–23] bending, ring on ring [24,25], and ball-on-ring (BoR) [26–28] have been developed for studying the strength properties of different PZT. Assuming that a crack originates as a result of preexisting surface flaws in brittle materials, biaxial flexure loading techniques, such as BoR

☆This manuscript has been authored by UT-Battelle LLC under Contract no. DE-AC05-00OR22725 with the US Department of Energy. The United States Government retains and the publisher, by accepting the article for publication, acknowledges that the United States Government retains a non-exclusive, paid-up, irrevocable, world-wide license to publish or reproduce the published form of this manuscript, or allow others to do so, for United States Government purposes.

*Corresponding author. Tel.: +1 865 574 5601; fax: +1 865 574 6098.
E-mail address: wangh@ornl.gov (H. Wang).

0272-8842/$ - see front matter © 2012 Elsevier Ltd and Techna Group S.r.l. All rights reserved.
http://dx.doi.org/10.1016/j.ceramint.2012.08.054

test, can be used to provide effective and reliable failure information on specimens with naturally occurring flaws.

Fracture behaviors of poled PZT subjected to either pure electrical or pure mechanical loading or a combination of both were investigated using the BoR biaxial flexure strength technique [26,27]. It was found that the characteristic strength depends on the electric loading conditions. A higher biaxial flexure strength value was observed at $+E_C$ (E_C, the coercive electric field), while a lower value was found at $-E_C$. Efforts have recently been made by the authors to study both the as-received and aged PZT under high electric fields in the range of $-3E_C$ and $+3E_C$ [28]. However, complete information regarding the mechanical responses of a poled PZT layer in increasingly higher fields such as $\pm 4E_C$ is lacking. Such data is important because current piezo stacks are designed to maximize the strain by using high electric field. The rated electric field of some PZT stacks has reached as high as $3E_C$ [29]. At the same time, the local field level can be enhanced substantially around defects or preexisting flaws, even though the external field is homogeneous throughout the PZT (for example, within a PZT stack that has a plate-through electrode or PTE configuration). Additional failure mechanisms can be triggered [30] by such an enhanced field. A thorough understanding of PZT failure mechanisms under electromechanical loading can help ultimately optimize the design of products.

In this work, the strength properties of as-received poled PZT were studied experimentally under high electric field with an extended field range ($\pm 4E_C$). Tests were conducted at room temperature through a BoR setup with a controlled electric loading path. Electronic liquid FC-40 with a high dielectric strength was used to protect the setup from dielectric breakdown. Characteristic strength, Weibull modulus, and fracture toughness of as-received PZT were extracted. In the following, after an introduction to experimental approach, results and discussion on the effects of loading history, FC-40, and applied electric field magnitude will be presented.

2. Experimental approach

2.1. Materials and specimen preparation

The material used for this study was PZT PSI-5A4E (Piezo Systems Inc., Cambridge, MA), which was designated as an industry type PZT-5A (Navy Type II) piezoceramic. Main properties of PSI-5A4E from the manufacturer are listed in Table 1. This material was received as sheets 72.39 mm × 72.39 mm × 0.27 mm in size. Each PZT sheet was poled along the thickness direction, and both sides were coated with Ni electrodes (200 nm thick). A total of four sheets from the same purchase were used in this study. Each sheet was cut into plates 10.00 mm × 10.00 mm in size. To minimize the effect due to variation from sheet to sheet, these plates were randomly mixed and then grouped. 12 groups with twelve plates in each group were prepared for testing.

Table 1
Material properties of PZT PSI-5A4E[a].

	Symbol	Unit	Value
Dielectric constant		–	1800
Piezoelectric coefficients	d_{31}	pC/N	−190
	d_{33}	pC/N	390
Coercive field	E_C	kV/mm	1.20
Elastic modulus	C_{11}	GPa	66
	C_{33}	GPa	52
Poisson's ratio	υ	–	0.23
Curie temperature	T_c	°C	350

[a]Based on data sheet supplied by the manufacturer.

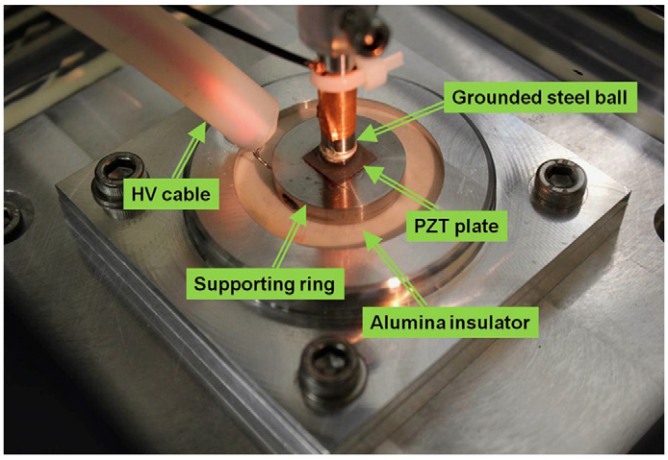

Fig. 1. BoR setup for high electric field coupled with mechanical loading testing. The steel ball is grounded while the cable is connected to a high-voltage amplifier (Trek model 609E-6, Medina, NY), which is not shown.

2.2. Experimental setup

The main part of the BoR (ball-on-ring) setup for application of a high electric field coupled with mechanical loading is shown in Fig. 1. A semi-sphere steel loading ball with a diameter of 6.45 mm was used. The steel supporting ring had an inner diameter of 7.44 mm, an outer diameter of 25.00 mm, and a thickness of 6.35 mm. The loading ball can be controlled to move vertically with the speed ranging from 0.001 mm/s to 1 mm/s. An amplifier with the capability of monitoring electric voltage and current in the operation range of ±4 kV was used. Electronic liquid FC-40 with dielectric strength of 18 kV/mm was used to prevent dielectric breakdown of the setup under high electric field. Two computers were used in this setup: one for controlling the electric loading and recording the voltage, current and charge, while the other for controlling the mechanical loading and recording the mechanical load exerted on the PZT plate.

2.3. Experimental procedures

Before a test, the PZT specimen and the supporting ring were carefully aligned with the loading ball to provide desired loading. A triangular waveform was used for controlling the electric loading path whose peak values were $\pm 4E_C$ or ± 4.80 kV/mm. The period of the waveform was defined by the peak field levels and electric loading and unloading rates, namely, ± 1.78 kV/mm/s. For a specified electric level or point on the defined path, twelve mechanical tests were carried out in order to generate one group of data. In this study, eleven combinations of electromechanical loading were considered as shown in Fig. 2, including the OC (open circuit) condition in $G1$. The electric loading in each test was started at zero, then ramped onto a specified field level, and finally held at that level for mechanical loading. The mechanical loading was initiated 10 s later with a crosshead speed of 0.001 mm/s. An additional group ($G12$) of specimens was tested in air at OC to investigate if there was any effect of the electronic liquid on the flexural strength.

Fracture stress was calculated using contact stress theory [31,32,28]. Weibull analysis software (WeibPar, Connecticut Reserve Technologies, Inc., Strongsville, OH) was used to analyze the strength data sets obtained. Unbiased maximum likelihood parameter estimation was used for these parameters as recommended by ASTM Standard C1239-00 [33]. In this study, 2-parameter Weibull strength distribution was chosen to characterize the strength distribution of the tested PZT-5A, and the corresponding equation is given by

$$P_f = 1 - \exp\left[-\left(\frac{\sigma_f}{\sigma_\theta}\right)^m\right], \quad (1)$$

where P_f is the probability of failure, σ_f is the fracture stress that is the maximum stress at failure, σ_θ is the characteristic strength, and m is the Weibull modulus [34]. Lastly, the fracture surfaces of the tested specimens were examined via optical microscopy (Nikon Nomarski Measure Scope MM-11, Tokyo, Japan) and scanning electron microscopy (SEM, Hitachi S4800 field emission scanning electron microscope, San Jose, CA). The strength limiting flaws were identified and further correlated to the fracture stresses of the specimens through apparent fracture toughness. It has been observed that strength limiting flaws are mostly surface-located and could be modeled as a semi-elliptical surface crack [27,28]. The apparent fracture toughness K_{IC} of the PZT was thus estimated by

$$K_{IC} = Y\sqrt{a}\sigma_f, \quad (2)$$

where a is the crack size that equals to the depth of surface-located flow. Y is a stress intensity geometry factor and is related to stress state, specimen, and crack geometry as will be discussed in the following.

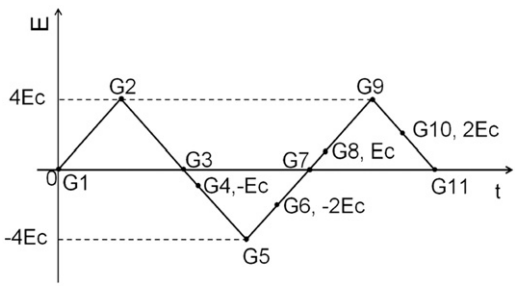

Fig. 2. Electric loading path for the BoR testing.

3. Experimental results and discussion

3.1. Effect of electric loading history on the flexural strength

No dielectric breakdown was observed for all the tested PZT specimens in this study, even though the electric field reached as high as $\pm 4E_C$. Therefore, the electronic fluid (FC-40) has effectively eliminated the partial discharges that existed in the previous study [28].

Weibull plots based on the WeibPar output are shown in Fig. 3(a), (c), and (e) for zero or OC, positive and negative electric field conditions respectively, in which estimates of characteristic strengths and Weibull moduli are given as well; the 95% confidence ratio rings of the data sets are shown in Fig. 3(b), (d), and (f) correspondingly. It can be seen that strength data sets under OC or zero field condition overlap to a large extent and are located in a narrow strength range (120∼160 MPa). It should be noted that the electric field condition was actually similar among the specimens of OC ($G1$) and zero field ($G3$, $G7$ and $G11$) groups, considering that the residual field in a poled PZT specimen under OC condition is generally negligible. Nevertheless, the loading cycles involved of $G1$, $G3$, $G7$, and $G11$ were different as shown in Fig. 2. The overlapping confidence ratio rings of the data sets means that the number of electric cycles is not a major factor within the test range as long as a zero field is reached. Similar observation holds for the $4E_C$ data sets ($G2$ and $G9$) in which nearly identical data boundaries and almost fully overlapping confidence ratio rings were seen, even though the $G9$ experienced an additional cycle.

Results for the flexural strength of the PZT-5A specimens tested in this study (Mix*) and in the previous study (Mix#) are summarized in Table 2. It is worth noting that no loading path was involved in the Mix#; namely, the electric field was ramped directly from OC to a designed level and held for subsequent mechanical loading. The data sets of $G1$, $G3$, $G7$, $G11$, and $G12$ were pooled because the OC data sets were not statistically different. Same pooling process was also applied to the $4E_C$ data sets ($G2$ and $G9$). The pooled data sets were then reevaluated and the parameters re-estimated. Weibull plots based on both Mix* and Mix# at OC, $-E_C$, and E_C are shown in Fig. 4(a), where Pooled^{OC}, $G4$, and $G8$ were selected from Mix* to represent respective electric conditions. Strength results under the $-E_C$, OC, and E_C conditions are shown to be

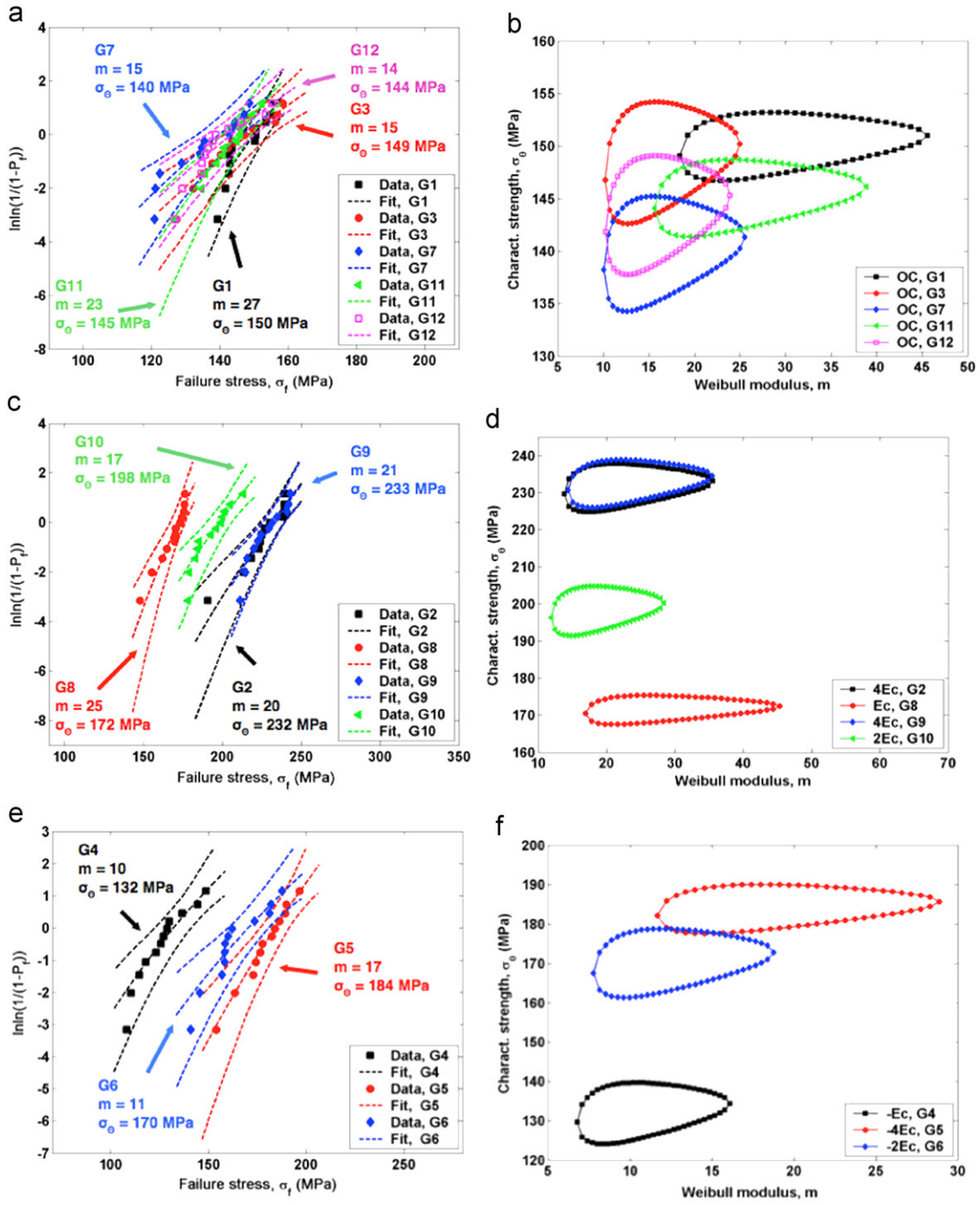

Fig. 3. Weibull plots for the flexure strength as well as the corresponding 95% confidence ratio rings of the as-received PZT-5A with zero field or OC (a) and (b), positive electric fields (c) and (d), and negative electric fields (e) and (f).

located from left to right as expected for both Mix* and Mix#. However, at the same electric load, no significant overlapping was observed between the data sets of Mix* and Mix#. Such observation is obviously consistent with the 95% confidence ratio rings as demonstrated in fig. 4(b). The rings corresponding to $-E_C$, OC, E_C for the specimens from sheet Mix# and Mix* are isolated and orderly located from bottom to top.

A detailed examination showed that specimens from sheet Mix* had a higher strength level than the ones from Mix# under designed load levels. Such difference at $-E_C$ was substantially remarkable with a level as high as 21 MPa. The similarity of PZT's fabrication of both the Mix* and Mix# was validated by the overlapping intervals of OC (in air) Weibull modulus and characteristic strength (Table 2). Therefore, the increase observed above in the

Table 2
Weibull analysis results for poled PZT PSI-5A4E.

Specimens	No. of tests	Designated load (E_C)	Medium	Weibull modulus	Interval (95%)	Char. strength (MPa)	Interval (95%)
Mix*(*G*1)	12	0	FC-40	27	18, 46	150	147, 153
Mix*(*G*3)	12		FC-40	15	10, 25	149	143, 154
Mix*(*G*7)	12		FC-40	15	10, 26	140	134, 145
Mix*(*G*11)	12		FC-40	23	16, 39	145	141, 149
Mix*(*G*12)	12		Air	14	10, 24	144	138, 149
Mix#	12		Air	29	19, 50	137	134, 140
Pooled^{OC}	60		FC-40; Air for *G*12	17	14, 21	146	144, 148
Mix*(*G*4)	12	−1	FC-40	10	7, 16	132	124, 140
Mix#	12		Air	23	17, 39	111	108, 113
Mix*(*G*6)	12	−2	FC-40	11	8, 19	170	161, 179
Mix*(*G*5)	12	−4	FC-40	17	12, 29	184	178, 190
Mix*(*G*8)	12	1	FC-40	25	17, 45	172	168, 175
Mix#	12		Air	12	8, 21	159	151, 167
Mix*(*G*10)	12	2	FC-40	17	12, 28	198	191, 205
Mix*(*G*2)	12	4	FC-40	20	14, 36	232	224, 237
Mix*(*G*9)	12		FC-40	21	14, 36	233	226, 239
Pooled^{4EC}	24	4	FC-40	22	17, 32	232	228, 236

Pooled^{OC} is based on data sets of Mix*; namely, *G*1, *G*3, *G*7, *G*11, and *G*12; Mix# denotes the as-received specimens from sheet 5–8 [28]; Mix* denotes the as-received specimens from sheet 9–12 in the current study.

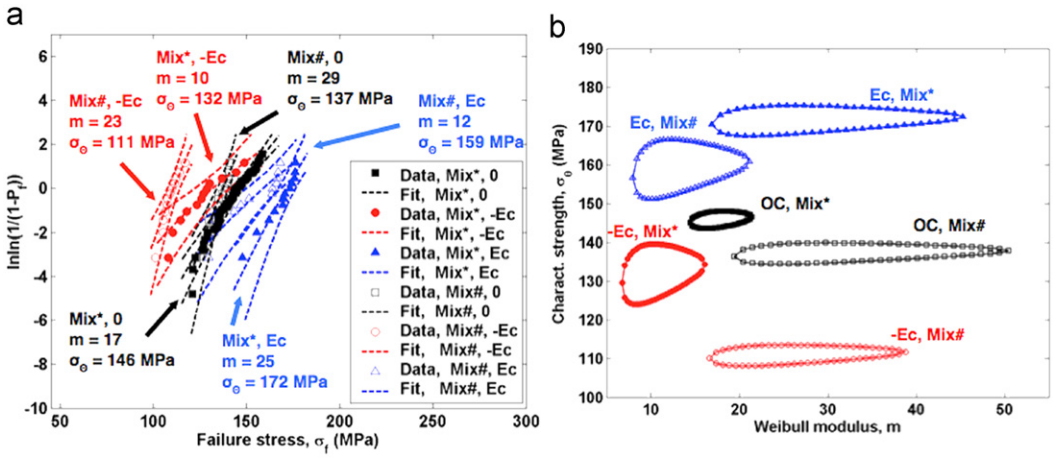

Fig. 4. Weibull plots for the flexure strength of (a) as-received PZT-5A of Mix* (Pooled^{OC}, *G*4, *G*8) and Mix# [28] tested under OC, $+E_C$, and $-E_C$, and (b) the 95% confidence ratio rings.

strength of Mix* should signify the impact of loading history on mechanical response of PZT. A half cycle to $4E_C$ was shown to have introduced substantial poling effect on the *G*4 of Mix*. More switchable non-180° domains [35,36] sustained the depolarization at $-E_C$ than that of Mix# without the half cycle but directly loaded to $-E_C$. Such non-180° domains play a vital role in the switching toughening [27,28].

3.2. Effect of electronic fluid on the flexural strength

Disregarding the fatigue effect, the characteristic strength for *G*1, *G*3, *G*7, and *G*11 should be the same theoretically. In fact, no statistically significant difference was seen among these strength data sets as mentioned above. By taking an average of the four strength data, a mean strength value of 146 MPa was obtained. Comparing the mean strength value with the strength value of *G*12 (144 MPa) shows that the FC-40 has little effect on the flexure strength testing.

3.3. Effect of electric field on the flexural strength

Strength data under E_C (*G*8), $2E_C$ (*G*10), and $4E_C$ (*G*2 and *G*9) conditions are shown from left to right in Fig. 3(c). Similarly, strength data under $-E_C$ (*G*4), $-2E_C$ (*G*6), and $-4E_C$ (*G*5) conditions are distributed from left to right in Fig. 3(e). It was again found that flexural strength of the specimens depended on both the magnitude and the direction of electric field. Disregarding the sign, the rings with higher electric field strength are located at higher strength levels. However, for the same electric field strength magnitude, the rings with positive

electric field are located higher than those with negative electric field.

Fig. 5 shows the characteristic strength of the tested specimens plotted as electric field strengths. The data of as-received PZT-5A from sheet 5–8 or Mix# obtained from the previous study [28] were also plotted in the figure. An asymmetry "V" curve was observed for both Mix* and Mix#, and the bottom of "V" curve was located near the negative coercive field. Though a similar trend was observed for these two sets of data, the strengths of PZT-5A from different sheets for the same electric load are different. The strength difference between Mix* and Mix# was significant under $-E_C$ and becoming larger at high positive electric field.

More scattered strength (i.e. low Weibull modulus) and fracture toughness data were obtained at negative electric field region. This could be caused by the formation of microcracks during the domain switching process. In addition, the growth of preexisting flaws might take place in PZT.

3.4. Strength limiter and fracture toughness

Scanning electron microscopy (SEM) studies showed that the failure origins or the strength-limiting flaws of interest are all inherently located near the tensile surface of the specimen in the BoR configuration, and the fracture surfaces of the tested PZT-5A were dominated by both intergranular and transgranular fracture. Fig. 6 is a SEM image showing one of these fracture surfaces in which the volume-distributed agglomerate can be seen as a failure origin near the tensile face of the flexure specimen. All the flaws of the tested PZT were observed to be in semi-penny shapes.

The extensive fractographical study showed that the crack depths were similar in all tested conditions with an average value of 18 μm. Using Eq. (2) discussed in Section 2.3,

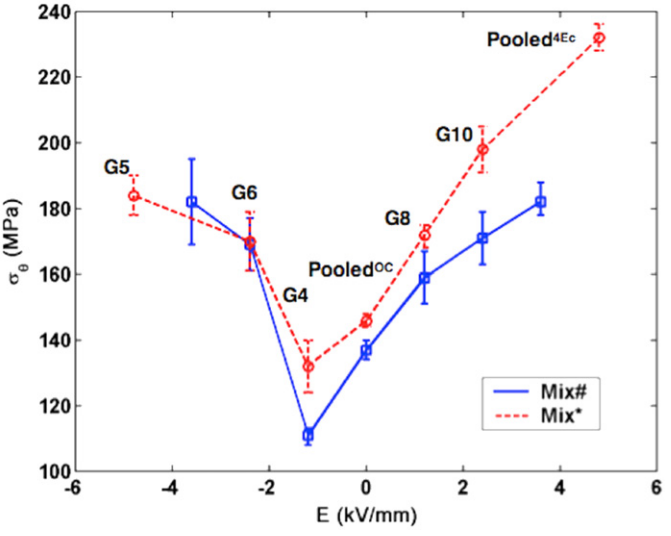

Fig. 5. Relations between the characteristic strength (σ_θ) and the electric field (E); the error bars correspond to 95% confidence intervals. Data for Mix# were taken from the previous study [28].

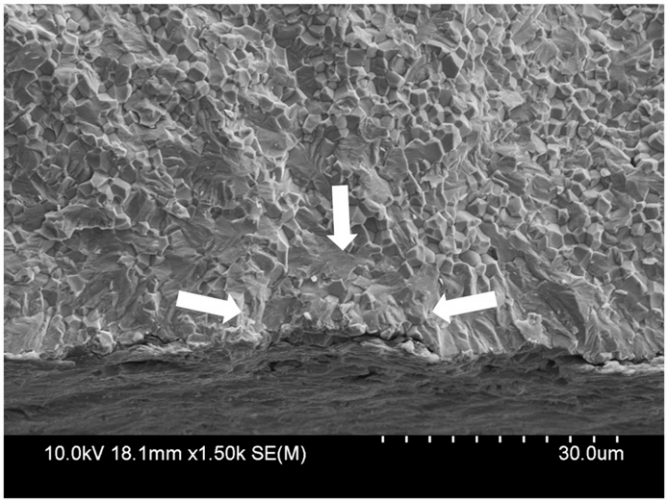

Fig. 6. SEM image of a fracture surface showing the failure origin of a PZT plate tested under $4E_C$; the failure stress is 237 MPa. The arrows indicate the failure origin.

Table 3
Summary of K_{IC} values (MPa m$^{1/2}$) of PZT PSI-5A4E.

Specimens	E (kV/mm)	Experimental results[a]
Mix* (*G5*)	−4.80	1.00 ± 0.07
Mix* (*G6*)	−2.40	0.93 ± 0.08
Mix* (*G4*)	−1.20	0.62 ± 0.07
Mix#		
Mix* (*G1*)		
Mix* (*G3*)		
Mix* (*G7*)	OC	0.76 ± 0.05
Mix* (*G11*)		
Mix* (*G12*)		
Mix#		
Mix* (*G8*)	1.20	0.87 ± 0.08
Mix#		
Mix* (*G10*)	2.40	0.94 ± 0.06
Mix* (*G2*)	4.80	1.26 ± 0.07
Mix* (*G9*)		

[a]Deviations of estimate correspond to 95% confidence intervals.

where Y was estimated to be 1.29 with respect to the crack semi-axis-to-depth ratio [37], an estimate of the fracture toughness can be made with the incorporation of the fracture stresses. Average results under a specified electric condition are summarized in Table 3.

Fracture toughness was found to be different for different electric field conditions. The specimens tested under an electric field magnitude of 1.2 kV/mm ($+E_C$) showed a higher strength level than those tested without applying an electric field; the application of electric field of 1.2 kV/mm could introduce more switchable non-180° domains in the field direction. Since some of the non-180° domains were not aligned along the stress direction and these domain activities are constrained locally, high compressive stress was developed near the crack tip to compensate the tensile stress and thus enhanced the

fracture toughness. On the other hand, when considering that a pre-loaded electric field is opposite to the polling direction, PZT can either be re-poled in the opposite direction or weakened in terms of polarization. The reason why PZT did not undergo any toughening at -1.2 kV/mm ($-E_C$) was because its polarization value was lower than the initial polarization value, which indicated the PZT specimens behaved as if un-poled after electric loading. Even though $-E_C$ could also result in non-180° or 90° domain switching in theory [35,36], not enough domain activities were available to develop a compressive stress near the crack tip. Furthermore, an increase in electric field strength in either direction and the relatively slow loading rates would re-polarize the specimens and force more unfavorable domains (including 180° and non-180° domains) to align along the field direction, which results in higher fracture toughness. However, with a further increase in electric field strength, the switchable non-180° domains lessened. Consequently, the enhancement rate of fracture toughness was slowed down until it reached saturation state. This effect is most obvious in the negative electric field region; characteristic strength under the positive electric field region still has a tendency to increase, which means that the saturation state under positive electric field is higher than $4E_C$. This was confirmed by Fig. 5 and the calculated fracture toughness as shown in Table 3.

4. Conclusions

Based on the experimental results under BoR testing, the following conclusions are made.

1. Mechanical strength of the as-received poled PZT depended on the sign, magnitude, and path of the applied electric field.
2. Within the examined electric field range of $-4E_C$ to $4E_C$, mechanical strength deceased initially with increasing electric field, reached the bottom at $-E_C$, and started increasing rapidly. Such "V" shaped curve existed in the electric loading cases with and without controlled loading path.
3. For the same electric field magnitude, the PZT under positive electric field had higher strength than those tested under a negative electric field. Therefore, the "V" curve was not symmetrical just as the bottom of "V" curve was not located at the zero electric field point.
4. No dielectric breakdown was observed when testing under electronic fluid FC-40, and it was shown that FC-40 had little effect on the flexure strength testing.
5. Surface-located volume-distributed flaws were identified to be strength-limiting flaws for this PZT material.
6. "V" curves with and without controlled electric loading path crossed near $-2E_C$. The lowered increasing rate of mechanical strength below $-2E_C$ and substantial strength increase beyond $-2E_C$ may involve a toughness saturation process, but it remains to be investigated further.

Acknowledgments

The authors are grateful to Drs. Michael Lance and Fei Ren for reviewing the manuscript and giving useful suggestions. This research was sponsored by the US Department of Energy, Office of Energy Efficiency and Renewable Energy, Vehicle Technologies Program, as part of the Propulsion Materials Program under contract DE-AC05-00OR22725 with UT-Battelle, LLC.

References

[1] C.A. Randall, A. Kelnberger, G.Y. Yang, R.E. Eitel, T.R. Shrout, High strain piezoelectric multilayer actuators: a material science and engineering challenge, Journal of Electroceramics 14 (2005) 177.
[2] H. Meixner, Technology of the future, EPCOS Components, Direct Link 1010, ⟨www.epcos.com⟩, 2006.
[3] K. Uchino, Piezoelectric Actuators and Ultrasonic Motors, Kluwer Academic Publishers, Norwell, MA, 1997.
[4] W. Yang, F. Fang, Toughening of ferroelectrics by the out-of-plane poling, Acta Mechanica Sinica 19 (2) (2003) 147–153.
[5] H. Aburatani, S. Harada, K. Uchino, A. Furuta, Y. Fuda, Destruction mechanisms in ceramic multilayer actuators, Japanese journal of Applied Physics 33 (5B) (1994) 3091–3094.
[6] C. Schuh, T. Steinkopff, A. Wolff, K. Lubitz, Piezoceramic multilayer actuators for fuel injection systems in automotive area, in: C.S. Lynch (Ed.), Smart Structures and Materials 2000: Active Mater.: Behavior and Mechanics, Proceedings of SPIE, Vol. 3992, , 2000, pp. 165–175in: C.S. Lynch (Ed.), Smart Structures and Materials 2000: Active Mater.: Behavior and Mechanics, Proceedings of SPIE, Vol. 3992, 2000, pp. 165–175.
[7] J. Pritchard, C.R. Bowen, F. Lowrie, Multilayer actuators: review, British Ceramic Transactions 100 (6) (2001) 1–9.
[8] K. Mehta, A.V. Virkar, Fracture mechanism in ferroelectric-ferroelastic lead zirconate titanate (Zr:Ti=0.54:0.46) ceramics, Journal of the American Ceramic Society 73 (3) (1990) 567–574.
[9] A.G. Tobin, Y.E. Pak, Effects of electric field on fracture of piezoelectric ceramics, Proceedings of SPIE Smart Structures and Materials 1916 (1993) 78–86.
[10] P. Monica, M.Jose Calderon–Moreno, Indented crack growth during poling of a high displacement PZT material, Materials Science and Engineering: A 319–321 (2001) 697–701.
[11] R. Fu, T.Y. Zhang, Effects of an electric field on the fracture toughness of poled lead zirconate titanate ceramics, Journal of the American Ceramic Society 83 (5) (2000) 1215–1218.
[12] S.L. dos Santos e Lucato, D.C. Lupascu, J. Rödel, Effect of poling direction on *r*-curve behavior in lead zirconate titanate, Journal of the American Ceramic Society 83 (2) (2000) 424–426.
[13] W.S. Oates, C.S. Lynch, Subcritical crack growth in lead zirconate titanate, Journal of the American Ceramic Society 87 (7) (2004) 1362–1364.
[14] T. Fett, G. Martin, D. Munz, *v–K* curves for borosilicate glass obtained from static bending tests with cracks introduced by the bridge method, Journal of Materials Science Letters 10 (4) (1991) 220–222.
[15] R. Fu, C.F. Qian, T.Y. Zhang, Electrical fracture toughness for conductive cracks driven by electric fields in piezoelectric materials, Applied Physics Letters 76 (1) (2000) 126–128.
[16] Y. Shindo, H. Murakami, K. Horiguchi, F. Narita, Evaluation of electric fracture properties of piezoelectric ceramics using the finite element and single-edge precracked-beam methods, Journal of the American Ceramic Society 85 (5) (2002) 1243–1248.
[17] F. Fang, W. Yang, Poling-enhanced fracture resistance of lead zirconate titanate ferroelectric ceramics, Materials Letters 46 (2–3) (2000) 131–135.

[18] H.T. Huang, P. Hing, Nonlinear stress–strain behaviour and stress relaxation of PZFNTU ceramics in the three-point bending test, Journal of Physics D: Applied Physics 33 (2000) L33–L37.
[19] F. Narita, Y. Shindo, F. Saito Cyclic, Fatigue crack growth in three-point bending PZT ceramics under electromechanical loading, Journal of the American Ceramic Society 90 (8) (2007) 2517–2524.
[20] H. Makino, N. Kamiya, Effect of dc electric field on mechanical properties of piezoelectric ceramics, Japanese Journal of Applied Physics 33 (9B) (1994) 5323–5327.
[21] T. Fett, D. Munz, G. Thun, Bending strength of a PZT ceramic under electric fields, Journal of the European Ceramic Society 23 (2) (2003) 195–202.
[22] A. Kolleck, G.A. Schneider, F.A. Meschker, Curve behavior of $BaTiO_3$ and PZT ceramics under the influence of an electric field applied parallel to the crack front, Acta Materialia 48 (16) (2000) 4099–4113.
[23] C.R.J. Salz, M. Hoffman, I. Westram, J. Rodel, Cyclic fatigue crack growth in PZT under mechanical loading, Journal of the American Ceramic Society 88 (5) (2005) 1331–1333.
[24] L.V. Zhoga, V.V. Shpeizman, Failure of ferroelectric ceramics in electric and mechanical fields, Soviet Physics—Solid State 34 (1992) 2578–2583.
[25] M.G. Cain, M. Stewart, M.G. Gee, Mechanical and electric strength measurements for piezoelectric ceramics: technical measurement notes, NPL REPORT CMMT (A) 99 (1998).
[26] H. Wang, A.A. Wereszczak, Effects of electric field on the biaxial strength of poled PZT, Ceramic Engineering and Science Proceedings 28 (8) (2007) 57–67.
[27] H. Wang, A.A Wereszczak, Effects of electric field and biaxial flexure on the failure of poled lead zirconate titanate, IEEE Transactions on Ultrasonics, Ferroelectrics and Frequency Control 55 (12) (2008) 2559–2570.
[28] H. Wang, H.T. Lin, A.A. Wereszczak, Strength Properties of poled lead zirconate titanate subjected to biaxial flexural loading in high electric field, Journal of the American Ceramic Society 93 (9) (2010) 2843–2849.
[29] 〈http://www.noliac.com/Plate_stacks-59.aspx〉, (accessed 05.01.12).
[30] X. Tan, J.K. Shang, In-situ transmission electron microscopy study of electric-field-induced grain boundary cracking in lead zirconate titanate, Philosophical Magazine A 82 (8) (2002) 1463–1478.
[31] R.J. Roark, W.C. Young, Formulas for Stress and Strain, fifth ed., McGraw-Hill, New York, 1975, pp. 366–513.
[32] A.F. Kirstein, R.M. Woolley, Symmetrical bending of thin circular elastic plates on equally spaced point supports, Journal of Research of the National Bureau of Standards 71C (1) (1967) 1–10.
[33] ASTM Standard C1239-00, Standard Practice for Reporting Uniaxial Strength Data and Estimating Weibull Distribution Parameters for Advanced Ceramics, vol. 15.01, ASTM, West Conshohocken, Pennsylvania, 2002.
[34] W. Weibull, A statistical distribution function of wide applicability, Journal of Applied Mechanics 18 (1951) 293–298.
[35] S. Li, A.S. Bhalla, R.E. Newnham, L.E. Cross, 90° domain reversal in $Pb(Zr_xTi_{1-x})O_3$ ceramics, Journal of Materials Science 29 (5) (1994) 1290–1294.
[36] P.M. Chaplya, G.P. Carman, Dielectric and piezoelectric response of lead zirconate-lead titanate at high electric and mechanical loads in terms of non-180° domain wall motion, Journal of Applied Physics 90 (10) (2001) 5278–5286.
[37] J.C. Newman, I.S. Raju, An empirical stress-intensity factor equation for the surface crack, Engineering Fracture Mechanics 15 (1–2) (1981) 185–192.